Perot devices can be designed with just a single-layer membrane suspended over a substrate that, therefore, have the same wide manufacturing tolerances and low finesse (and thus broad spectral bandwidth) as the MARS device.

Fabry-Perot devices are typically designed such that the mirrors have equal reflectivity and opposite phase. Then the condition for zero overall reflectivity is that the air gap be $\lambda/2$, because with a total round trip of λ, the reflectivities of the top and bottom mirror add destructively. As shown below, in designing a micromechanical modulator consisting of a single-layer membrane suspended over the substrate, using this design principle, one simply recovers the MARS principle that $n = n_s^{1/2}$ and $t = \lambda/(4n)$.

However, if one examines the basic equation of the Fabry-Perot etalon,[8] phases not exactly opposite are compensated for by using an air gap different than $\lambda/2$. The reason to explore such phase-mismatched Fabry-Perot (PFP) devices is that it expands the range of refractive indices useful for the membrane. This allows higher index, lower stress silicon nitride or even poly-Si to be used as the membrane. This may be advantageous because the ply-Si can be doped so that the entire membrane is charged, thus lowering drive voltage.

Thus all that is necessary to design a Fabry-Perot device consisting of a single-layer membrane suspended over a substrate is that the magnitude of the reflectivities of the membrane and the substrate be equal. The (normal incidence) reflectivity of a dielectric slab of thickness t and refractive index n in air is given by

$$\rho = (1 - n^2)\sin(kt)/[(n^2 + 1)\sin(kt) + 2i\cos(kt)],$$

where $k = 2\pi n/\lambda$. The reflectivity of the substrate (index n_s) is given by $\rho_s = (n_s - 1)/(n_s + 1)$. Setting $\rho = -\rho_s$ would result in $kt = \pi/2 + m\pi$, $n = n_s^{1/2}$, and we recover the principle of the MARS.[1] However, our premise here is that phase-mismatched Fabry-Perot cavities can still achieve nulled overall reflectivity. If we set the magnitudes of ρ and ρ_s equal, any index $n > n_s^{1/2}$ allows a solution

$$kt = \pi/2 + m\pi \pm \tan^{-1}[(n^2 + 1)\cdot(f - 1)^{1/2}/(2n)],$$

$$f = [(n^2 - 1)/(n^2 + 1)]^2/[n_s - 1)/(n_s + 1)]^2.$$

The two solutions result from taking the square root of $(f - 1)$. The air gap (d) required to null the overall reflectivity is then modified from $\lambda/2$ due to the mismatch in the reflectivity phases of the membrane and the substrate:

$$d = \lambda/2\{1 \mp \tan^{-1}[(f - 1)^{1/2}]/(2\pi)\}.$$

In Fig. 2 the membrane thickness vs. index is shown for the PFP design, and in Fig. 3 the air gap vs. index is shown that achieve zero overall reflectivity. Note that the quiescent air gap of the device will probably be larger than d so that high reflectivity is achieved at zero bias. For any index $n > n_s^{1/2}$, there are two designs, a thinner membrane with a larger air gap, and a thicker membrane with a smaller air gap. The thinner membrane solution will probably have lower drive voltage due to larger compliance, and thus will be preferred as long as it has sufficient yield and reliability.

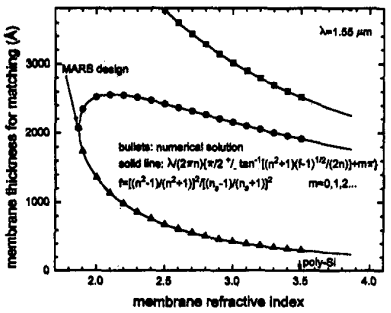

CTuW3 Fig. 2 Membrane thickness vs. refractive index for the phase-mismatched Fabry-Perot (PFP) design for a silicon substrate. There are two solutions for any refractive index greater than the square root of the substrate's.

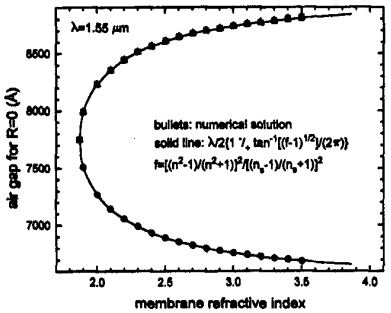

CTuW3 Fig. 3 Required air gap to achieve zero overall reflectivity for the PFP design vs. refractive index. For thin (thick) membrane solutions, the air gap is thicker (thinner). Note the quiescent air gap of the device will probably be larger so that the device has high reflectivity at zero bias.

In conclusion, we have presented an additional optical design for noncontacting substrate-air-membrane micromechanical modulators that improves upon the basic MARS by allowing a larger range of refractive indices to be used for the membrane.

AT&T Bell Laboratories, Murray Hill, New Jersey 07974

1. K. W. Goossen, J. A. Walker, S. C. Arney, IEEE Photon. Technol. Lett. **6**, 1119 (1994).
2. J. A. Walker, K. W. Goossen, S. C. Arney, N. J. Frigo, P. P. Iannone, Transducers '95-Eurosensors IX, 1995, Stockholm, Sweden, Royal Swedish Academy of Engineering Sciences, p. 285.
3. N. J. Frigo, P. Iannone, K. C. Reichmann, J. A. Walker, K. W. Goossen, S. C. Arney, E. J. Murphy, Y. Ota, R. G. Swartz, 1995 European Conference on Optical Communication, September, 1995, Brussels, Belgium.
4. K. Aratani, P. J. French, P. M. Sarro, R. F. Wolffenbuttel, S. Middelhoek, in Proceedings of IEEE Microelectromechanical Workshop, February 7–10, 1993, Fort Lauderdale, Florida, p. 230.
5. C. Marxer, M. A. Gretillat, V. P. Jaecklin, R. Baettig, O. Anthamatten, P. Vogel, N. F. de Rooij, Transducers '95-Eurosensors IX, 1995, Stockholm, Sweden, Royal Swedish Academy of Engineering Sciences, p. 289.
6. M. C. Larson, B. Pezeshki, J. S. Harris, Jr., IEEE Photon Technol. Lett. **7**, 382 (1995).
7. E. C. Vail, M. S. Wu, G. S. Li, L. Eng, C. J. Chang-Hasnain, Electron. Lett. **31**, 228 (1995).
8. H. A. Macleod, in *Thin-film optical filters*, W. T. Welford, Ed., (Adam Hilger, Bristol, Great Britain), p. 159.
9. J. A. Walker, K. W. Goossen, J. E. Cunningham, W. Y. Jan, D. A. B. Miller, J. Electron Mater. **23**, 1081 (1994).

CTuW4 **5:15 pm**

First monolithically integrated DBR waveguide laser and Mach-Zehnder intensity modulator in erbium-doped $LiNbO_3$

R. Corsini, D. Hiller, C. Carmannini, G. Consonni, S. Bosso, L. Gobbi, J. Söchtig,* H. Schütz,* R. Widmer,* *Pirelli Cavi SpA, DBT/RST/COS Viale Sarca 222, I-20126 Milano, Italy*

Free-running lasers, tunable lasers, modelocked lasers and distributed Bragg reflector (DBR) waveguide lasers have all been demonstrated in erbium-diffusion-doped $LiNbO_3$.[1,2] This paper reports on the first, to our knowledge, single-mode Er:$LiNbO_3$ DBR waveguide laser monolithically integrated with a Mach-Zehnder-type intensity modulator. This transmitter prototype is an attractive device for high-speed analog transmission and sensor applications.

The fabrication of the compact, single-chip, source/modulator device involves the following steps: a) planar doping of a Z-cut $LiNbO_3$ wafer close to the surface by indiffusion of erbium at 1100°C for 100 h in an oxygen atmosphere; b) transversal monomode stripe waveguide and Mach-Zehnder interferometer formation by a subsequent thermal diffusion of 6.5-μm wide, ~100-nm-thick titanium stripes at 1030°C for 9 h; c) creation of the laser cavity by dry etching a holographically defined 352.5-nm period first-order Bragg grating 300-nm deep into the $LiNbO_3$ surface and end-face deposition of a dielectric mirror stack of SiO_2/TiO_2 quarter-wave layers; d) deposition of a buffer layer and the traveling-wave Au-electrode outside the laser cavity on top of the Mach-Zehnder structure.

Figure 1 shows the layout of the la-

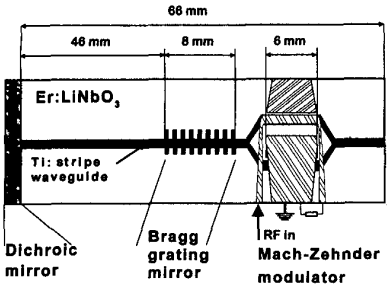

CTuW4 Fig. 1 Layout of the integrated laser/modulator sample.

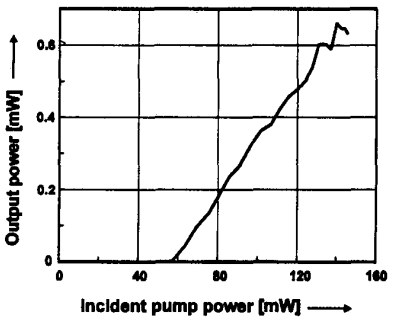

CTuW4 Fig. 2 Power characteristics of the optically pumped laser device.

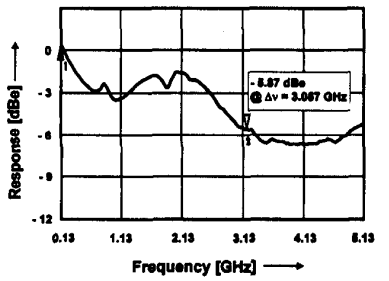

CTuW4 Fig. 3 Electro-optic bandwidth measurement of the combined laser/modulator.

ser/modulator configuration. The laser gain section between the 8-mm-long Bragg grating and the dichroic input coupler mirror is 46-mm long. Additional amplification is provided by the 12-mm-long erbium-doped waveguide section behind the laser cavity where the Mach-Zehnder interferometer is located.

The laser emission wavelength is adjusted by the Bragg grating period to λ_s = 1561.3 nm, where Er:$LiNbO_3$ has a local gain maximum. The Bragg mirror reflectivity exceeds 3.5 dB and the dichroic mirror shows a transmittance of 60% at the pump wavelength (λ_p = 1480 nm) and simultaneously a high reflectance (98%) at the laser emission wavelength (λ_s = 1561 nm). The device, pumped with a commercial fiber pigtailed semiconductor laser diode, has a threshold of 54.8-mW incident pump power and a slope efficiency of 0.69%; the maximum output power of 0.63 mW is obtained with 145-mW pump power under (σ)TE-polarized fiber butt coupling (Fig. 2). The small filter bandwidth of the Bragg mirror of <0.2 nm results in stable single-longitudinal-mode emission.

The measured serial resistance of the 6-mm-long travelling wave electrode is 10 Ω and the calculated RF impedance is 27 Ω. Figure 3 shows the frequency response with electro-optical modulation. The integrated laser/modulator device shows a bandwidth of 3.057 GHz at −6 dBe.

The authors gratefully acknowledge the support by the European Union within RACE II program (project R2013 EDIOLL) and the Swiss BBW (contract #92.005a).

Paul Sherrer Institute Zurich, Badenerstrasse 569 CH-8048 Zurich, Switzerland

1. R. Brinkmann, W. Sohler, H. Suche, Electron. Lett. **27**, 415–416 (1991).
2. J. Söchtig, R. Groß, I. Baumann, W. Sohler, H. Schütz, R. Widmer, Electron. Lett. **31**, 551–552 (1995).

CTuW5 **5:30 pm**

Integrated electroabsorption modulator/ DFB laser analog transmitter with distortion correction to fifth order

G. C. Wilson, T. H. Wood, J. L. Zyskind, J. W. Sulhoff, J. E. Johnson,* T. Tanbun-Ek,* P. A. Morton,* *AT&T Bell Laboratories, Crawford Hill Laboratory, Holmdel, New Jersey 07733-0400*

Interest in AM-VSB cable TV (CATV) systems operating at 1.55 μm with erbium-doped fiber amplifiers (EDFAs) is increasing rapidly. These systems provide high optical powers and enable large splitting ratios. The chirp produced by directly modulated DFB lasers at 1.55 μm leads to distortion in nondispersion-shifted fiber and in EDFAs with gain slope.[1] Integrated electroabsorption modulatd lasers (EMLs) have low chirp. Transmission through nondispersion-shifted fiber, without dispersion compensation and with negligible penalty, has recently been demonstrated, both using a linearized EML[2] and a linearized discrete electroabsorption modulator.[3] Simply biasing the modulator at the inflection point of its transmission-*vs.*-voltage curve produces low composite second-order distortion (CSO). The odd-order nonlinearity, parameterized by the composite-triple-beat (CTB), is high, however, and must be corrected by predistortion. In Ref. 2, 11.4 dB of third-order cancellation was achieved, yielding a CTB of −54.1 dBc. Typical specifications call for CTB ≤ −65 to −60 dBc. Here we report an improved predistorter, which cancels fifth-order (IMD5) as well as third-order (IMD3) intermodulation distortion and yields a CTB of −60 dBc. The uncorrected CSO is −61 dBc. The reduction in CTB (17.5 dB) is 6 dB better than the largest previously reported for an electroabsorption modulator. Low distortion is preserved after fiber amplification and propagation through 13 km of nondispersion-shifted fiber with a transmission-fiber launch power of +13.4 dBm.

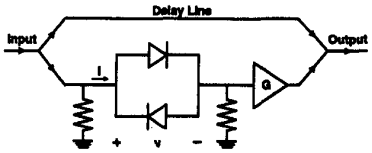

CTuW5 Fig. 1 Schematic of predistortion circuit.

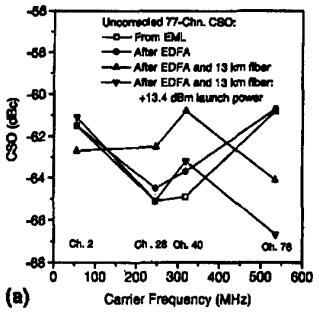

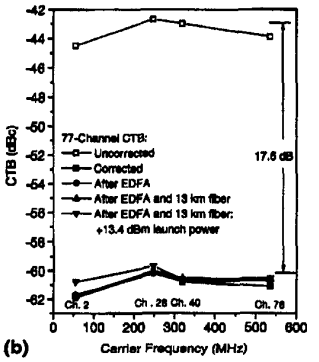

CTuW5 Fig. 2 (a) CSO and (b) CTB for 77 channels and OMD of 3.3% at four channels.

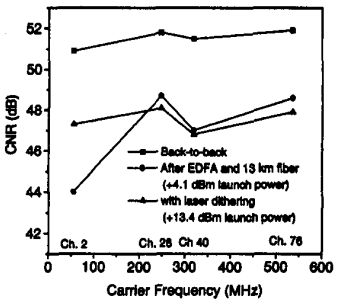

CTuW5 Fig. 3 CNR at various points in the link. The link CNR is shown with fiber launch power below the SBS threshold without laser dithering and above SBS threshold with laser dithering.

The electronic predistortion circuit is shown schematically in Fig. 1. The diode-pair has an odd-order $V - I$ impedance function. If the current through each diode is approximated by $I = I_0 \exp(V/V_T)$,